Transportation Research Interdisciplinary Perspectives 29 (2025) 101331

Contents lists available at ScienceDirect

Transportation Research Interdisciplinary Perspectives

journal homepage: www.sciencedirect.com/journal/transportation-research-interdisciplinary-perspectives

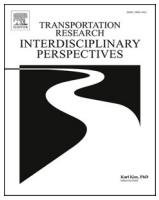

ANTi-JAM solutions for smart roads: Ant-inspired traffic flow rules under CAVs environment

Marco Guerrieri [a,*], Nicola Pugno [b,c]

[a] Department of Civil, Environmental and Mechanical Engineering, University of Trento, via Mesiano 77, 38123 Trento, Italy
[b] Laboratory for Bioinspired, Bionic, Nano, Meta Materials & Mechanics, Department of Civil, Environmental and Mechanical Engineering, University of Trento, Via Mesiano 77, 38123 Trento, Italy
[c] School of Engineering and Materials Science, Queen Mary University of London, Mile End Road, E1 4NS London, United Kingdom

ARTICLE INFO

Keywords:
Ant-Inspired Traffic
Deep learning
Traffic
Congestion
Platoons
Smart roads
CAVs

ABSTRACT

The behaviour of ants has inspired various scientific disciplines due to their ability to solve even complex problems. During their movement, ants generate trail networks that share many characteristics with vehicular traffic on highways. This research aims to estimate the values of traffic flow variables (mean speed, density, and flow) in ant trails without intersections or branches that could alter the dynamics of each ant. A case study in an outdoor environment was analyzed. The macroscopic traffic flow variables of interest were estimated using the deep learning method and the YOLO detection algorithm. The results show that ants adopt specific traffic strategies (platoon formation, quasi-constant speed and no overtaking maneuvers) that help avoid jam phenomena, even at high density. Emerging technologies, including smart roads, communication systems, and Cooperative and Automated Vehicles (CAVs), allow us to speculate on the use of traffic control systems inspired by ant behaviour to avoid the risk of congestion even at high traffic volumes, as demonstrated by the preliminary results of this research.

1. Introduction

Ants are the most common social insects, and their organization does not depend on a leader (Schadschneider and Chowdhury, 2011). The modelling of ant colony organization is used in various human fields, including computer science, communication engineering, artificial intelligence, micro-robotics, etc. (Schadschneider and Chowdhury, 2011). Ants belong to the class of eusocial insects and demonstrate a high degree of cooperation in transport processes (Holldobler and Wilson, 1990; Bonabeau et al. 2000) where collective movements are predominantly bidirectional with some degree of trail separation (Dussutour, 2004, Fig. 1). These insects are central-place foragers, which involves a series of trips from their nest to their foraging site. Many ant species generate chemical trail networks to transport resources and for exploration, emigration and coordinating colony defence (Holldobler and Wilson, 1990; Couzin and Franks, 2003). Each trail originates from a pheromone patch (Billen and Morgan, 1998) which creates a multi-component signal acting both as a recruitment and orientation signal (Fourcassié, et al. 2010). The flow rate of ants on a trail section can reach several hundred ants per minute (Poissonnier, et al., 2019). In terms of speed, ants move using a tripod gait with no more than three legs in the air at a time (Zollikofer, 1994; Reinhardt and Blickhan, 2014; Wang and Song, 2016), their running speed is a function of species, body size and surface type. Typical speed values range from about 1 cm/s to 10 cm/s depending on ant species and running surface (Grevé et al., 2019). The results of laboratory experiments show that the maximum ant density can reach 0.60 ants/cm and 0.95 ants/cm or more for large and small size ants, respectively (Wang and Song, 2016). Research on the organization of ant traffic has provided new insights for the study of pedestrians (Nishinari et al., 2006) and vehicular traffic (Peters et al., 2006). However, ants do not move like pedestrians or vehicles for the following reasons (Fourcassié, et al. 2010): i) ants moving along a foraging path come from the same colony, have a common goal, and work cooperatively to improve the group's overall fitness, which is not the case for pedestrians or drivers; ii) due to their low mass, ants have low inertia and therefore do not sustain damage in collisions. Consequently, some degree of mixing of opposing traffic streams on foraging trails is permissible. In general, the degree of lane separation of traffic streams is greater in ant groups characterized by large specimens than in those characterized by small specimens. Thus, ants can solve even difficult traffic regulation challenges through relatively simple rules that

* Corresponding author.
E-mail addresses: marco.guerrieri@unitn.it (M. Guerrieri), nicola.pugno@unitn.it (N. Pugno).

https://doi.org/10.1016/j.trip.2025.101331
Received 10 October 2024; Received in revised form 17 December 2024; Accepted 7 January 2025
Available online 13 January 2025
2590-1982/© 2025 The Author(s). Published by Elsevier Ltd. This is an open access article under the CC BY license (http://creativecommons.org/licenses/by/4.0/).

Nomenclature

A_c	Accuracy
a_i	acceleration of the i-th ant
c	theoretical stream capacity of CAVs
c_T	lane mean capacity value of a traditional highway
CAVs	Cooperative Automated Vehicles
C_i^j	confidence score of the j-th box in the i-th grid
D_s	space domain in the time–space plane
D_t	time domain in the time–space plane
D_{ts}	time/space domain in the time–space plane
ΔX	segment length (path length)
ΔT_j	j-th time interval observation of ant flow
FN	False Negative
FP	False Positive
g_{si}	space gap between the i-th and the (i + 1)-th ants
g_{ti}	time gap between the i-th and the (i + 1)-th ants
h_{si}	space headway between the i-th and the (i + 1)-th ants
h_{ti}	time headway between the i-th and the (i + 1)-th ants
h_{ti}^*	minimum value of the mean headway between CAVs
HVs	human-driving vehicles
IOU_{pred}^{truth}	degree of overlap between the predicted result and the bounding box in the original image
$k_{\Delta X}(t)$	ant density
k_c	critical density
k_{max}	maximum CAVs density
l	mean body length of an individual ant
L	observed track section of ants
l_i	ant's body length
Loss	loss function of the detection algorithm
m(t)	number of ants on the segment ΔX at the instant of time t
n(x)	number of ants that pass the cross-section x
P_r	precision
q(x)	(or q) flow rate measured in the cross-section x
q_{max}	maximum flow value of the traffic stream
R_e	recall
ρ_i	occupation time
t	time instant
TP	True Positive
TN	True Negative
t_{pr}	perception and reaction time of the driver
T	total time period of observation of ant flow
v_i	speed of the i-th ant
v_c	vehicles mean speed value related to the stream capacity
v_f	free-flow speed
v_{max}	maximum speed legally allowed on the highway
$\overline{v}_s(x)$	(or v) space mean speed
V2I	Vehicle-to-Infrastructure Communication Technology
V2V	Vehicle-to-Vehicle Communication Technology
x	cross-section of the ant's path
x_i	abscissa of the i-th ant
YOLO	object detection algorithm (acronym of You Only Look Once)

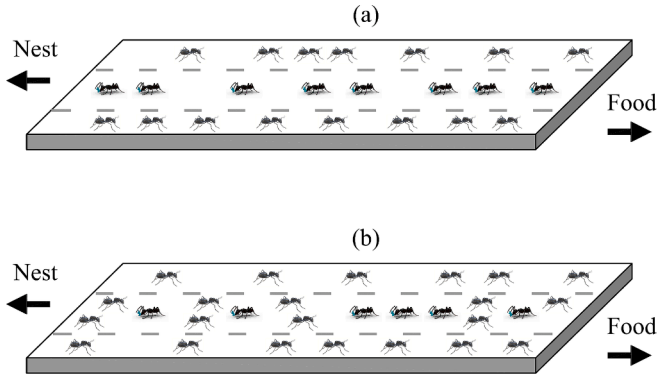

Fig. 1. Examples of the spatial organization of traffic flows. (a) the army ant Eciton burchelli (b) the leaf-cutting ant Atta Colombica (adapted from Fourcassié et al., 2010)

are not imposed externally (as in vehicle traffic flow regulated by signalized, unsignalized intersections and roundabouts (Gallelli et al., 2016; Gallelli and Vaiana, 2019; Guerrieri et al., 2015)) but result from direct interactions between specimens (i.e., direct contacts or pheromone trails). Nevertheless, ants generate trail systems during their motion that share many characteristics with traffic flows of highways and freeways. The main characteristics of traffic flows on ant trails have been empirically studied in previous research (Gallotti and Chialvo, 2018; John et al., 2008; Poissonnier et al., 2019).

In this paper, we apply specific traffic engineering models to analyse traffic parameters on bidirectional ant trails, which show striking correspondences with vehicle flows on highways under uninterrupted traffic conditions. The ant path considered is located in an outdoor environment and maintains a quasi-constant orientation over the observed time period, with no intersections or branches that could alter the dynamics of individual ants. Data were analysed in successive time intervals of 30 s each ($\Delta T_j = 30$ s), for a total observation period of 30 min ($T = \sum_j \Delta T_j = 30$ min). The length of the observed track section is L = 30 cm, which is approximately 100 times the mean body length l of an individual ant ($l \approx 3$ mm).

From ants walking on a pheromone trail to vehicles driving in a highway lane, the main challenge for all collective systems is to avoid congestion at high densities in crowded environments. Therefore, some of the key findings of this research on traffic ants could be applied to the development of traffic management and control systems for Cooperative Automated Vehicles (CAVs) on smart roads (Vidyarthi, et al., 2023). By self-organizing, the ants can maintain traffic flow close to the capacity of their trail without jamming. Similarly, on smart roads, the main challenge is to implement appropriate traffic control systems to maximize the capacity of traffic flows formed by CAVs and avoid congestion phenomena.

In short, the main novelties and contributions of this research are:

- deduce the microscopic traffic variable in ant streams;
- analysed the collective strategies used by ants to avoid congestion;
- suggest traffic regulation strategies inspired by ants' behaviour in smart roads used by CAVs to guarantee stable flow conditions even at high vehicle densities.

The structure of the paper is as follows. Section 2 describes the macroscopic flow variables of ant-traffic and the fundamentals of the car-following models and macroscopic traffic models derived from traffic engineering theory. Section 3 explains the related research on object detection and recognition systems based on the deep learning approach and the YOLOv4-Tiny detection algorithm, as well as the processes involved in ant detection and tracking. The experiments are presented in Section 4, along with the results and discussion. Finally, Section 5 provides conclusions, study limitations and research perspectives.

2. Ant-traffic: Macroscopic flow variables for and traffic models

The first assumption for analysing macroscopic traffic variables is the absence of overtaking manoeuvres among ants in a given traffic stream. Empirical data and previous research support this assumption which shows that ants may temporarily leave the initial path and be overtaken by subsequent ants but do not speed up to perform an overtaking manoeuvre (John et al., 2009) (see Section 4). Therefore, ants are individually identified by the order in which they cross a specific cross-section of the observed trail segment.

For a generic ant "i" the following variables can be defined (see Fig. 2a and Fig. 2b):

- body-length: l_i;
- abscissa x_i, (with respect to the x-axis coinciding with the axis of the trail);
- instantaneous speed: $v_i = \frac{dx_i}{dt}$ and longitudinal acceleration: $a_i = \frac{dv_i}{dt} = \frac{d^2x_i}{dt^2}$.

With respect to the direction of motion, we denote the leader ant with "i" and the follower ant with "i + 1". Therefore, between the two successive ants there is a space headway h_{si} and a time headway h_{ti} that can be defined as follows:

$$h_{si} = x_i - x_{i+1} = g_{si} + l_i \tag{1}$$

$$h_{ti} = g_{ti} + \rho_i \tag{2}$$

in which g_{si}, g_{ti} and ρ_i are the space gap, the time gap and the occupation time, respectively.

In addition, with respect to the time–space domain (cf. Fig. 2) the following macroscopic traffic variables can be estimated by means of counting processes:

- The *flow rate* or simply flow q(x) is the number of ants n(x) that pass the cross-section x , during the generic time interval ΔT, expressed in ants per time unit:

$$q(x) = \frac{n(x)}{\Delta T} \tag{3}$$

- *Space mean speed* $\overline{v}_s(x)$ is the *harmonic mean* of the instantaneous ant speeds $v_i(x)$ measured at the cross-section x, during the generic interval of time ΔT:

$$\overline{v}_s(x) = \frac{1}{\frac{1}{n}\cdot\sum_{i=1}^{n}\frac{1}{v_i(x)}} \tag{4}$$

- *ant density,* or simply, *density* $k_{\Delta x}(t)$, is the ant number m(t) on the segment ΔX long –expressed in ants per length unit- at the instant of time t:

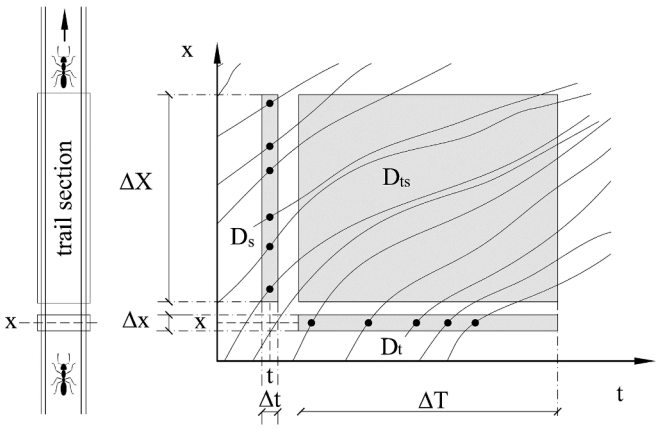

Fig. 3. Ants trajectories – space taken up in function of time (x = x(t)), by a group of ants, and identification of potential domains (D_t, D_s, D_{ts}) for analysing the flows.

$$k_{\Delta X}(t) = \frac{m(t)}{\Delta X} \tag{5}$$

For the sake of simplicity, in the next parts of this article, the macroscopic traffic flow variables are denoted as follows: flow q, space mean speed v and density k.

Strictly speaking, only in the case of steady-state traffic conditions (Mauro, 2014), the so-called fundamental flow relationship links the macroscopic flow variables (i.e. flow, density and space mean speed) to each other with the state equation:

$$q = k{\cdot}v \tag{6}$$

However, Eq. (6) is sometimes used in practical applications even in no steady-state traffic conditions.

To get an intuitive model for modelling ants' traffic, we can assume a linear response relation between a cause and the corresponding effect (i.e. Response ∝ Stimulus). In other words, the dynamics of ants can be modelled by their physical interactions and stimuli, according to the so-called car-following models of vehicular streams in which a vehicle driver responds to the generic stimulus at time t, induced by the driving speed of the preceding vehicle, accelerating or decelerating after a delay time $t + t_{pr}$ (t_{pr} is the perception and reaction time of the driver) and proportional to the result of the stimulus multiplied by the driver's sensitivity [1]:

$$\text{Response}(t + t_{pr}) = \text{sensitivity}{\cdot}\text{stimulus}(t) \tag{7}$$

In linear car-following models, the stimulus is a function of the speed difference between two vehicles in a platoon, whereas the sensitivity assumes a different form according to the selected model. Consider the lead vehicle "i" and the follower vehicle "i + 1", and assuming for the sensitivity a coefficient λ (e.g. the reciprocal value of the perception-

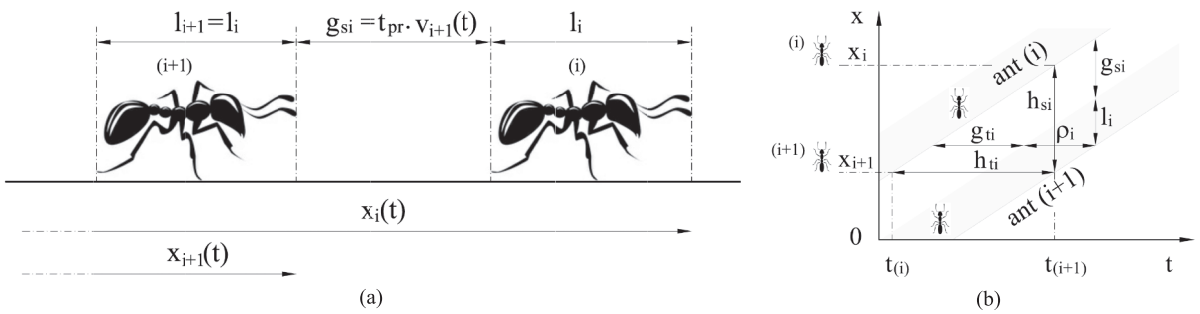

Fig. 2. Space and time headways between ants in a platoon.

reaction time t_{pr} of users), the linear car-following model is expressed as follows:

$$a_{i+1}(t+t_{pr}) = \lambda \cdot [v_i(t) - v_{i+1}(t)] \quad (8)$$

where $([v_i(t)\text{-}v_{i+1}(t)])$ is the speed difference between the lead vehicle "i" and the follower vehicle "i + 1" and $a_{i+1}(t+t_{pr})$ is the acceleration of the follower vehicle.

In the non-linear car-following model, the sensitivity λ is a function of the speed and spacing between vehicles; the model is expressed by the following equation:

$$a_{i+1}(t+t_{pr}) = \lambda_0 \cdot v_{i+1}^{m}(t+t_{pr}) \cdot \frac{v_i(t) - v_{i+1}(t)}{[x_i(t) - x_{i+1}(t)]^l} \quad (9)$$

Several non-linear models are available in the literature (e.g. Helly, 1961; Gabard et al., 1982; Gipps 1981; Bekey et al., 1977). It should be noted that macroscopic traffic models can be derived directly from the non-linear car-following model by assuming certain values of the coefficients m and l, as shown in Table 1 (Papageorgiou, 1991; Mauro, 2014). This study used the Greenshields model (Table 1) to analyze ant flows because it is the most popular model in traffic engineering applications.

3. Ants' detection and tracking in video sequences

In this research, we studied bidirectional ant traffic on a natural trail. A deep learning-based approach, utilizing the YOLOv4-Tiny algorithm, was applied to detect and track ants in an outdoor environment from recorded videos. In computer vision applications, the most commonly used Deep learning architectures are artificial neural networks (ANNs), convolutional networks (CNNs) and generative adversarial networks (GANs) (Elgendy, 2020). YOLO (You Only Look Once), SSD (single-shot detector) and Faster R-CNN are object detection methods capable of detecting, locating and classifying objects in images, including several object categories (Elgendy, 2020). YOLO is a powerful real-time object detection system first introduced by Redmon in 2016 (Redmon et al., 2016). In YOLO, the network divides an image into different regions and predicts bounding boxes and probabilities for each object of interest. The YOLO variants (i.e., YOLOv1, YOLOv2, YOLOv3, YOLOv4, YOLOv5,.. YOLOX, YOLOR) have complex network structures and a large number of network parameters, so a powerful GPU (Graphic Processing Unit) is required for real-time object detection. YOLO models play a key role in real-time object detection systems for robotics, driverless cars, and video monitoring applications (Terven and Córdova-Esparza, 2024). In traffic engineering, YOLO models have been applied for tasks such as traffic signs, structural distress, vehicular and pedestrian flow recognition (Guerrieri et al., 2013a; Guerrieri et al., 2013b), thus promoting the development of novel intelligent transportation systems and traffic management techniques. Compared to other one-stage and two-stage object detection methods, YOLOv4 shows better inference speed and detection performance in bounding box classification, prediction and generation (Liu et al., 2022; Zheng, et al., 2019; Li, et al. 2021).

Table 1
Some macroscopic flow models obtained from Eq. (9) through particular values of the coefficients m and l.

Coefficient values – Eq.(9) m	l	Traffic law	Denomination
0	1	$q = v_c \cdot k \cdot \ln\left(\frac{k_{jam}}{k}\right)$	Gazis et al. (1959)
0	1.5	$q = v_f \cdot k \cdot \left[1 - \left(\frac{k}{k_{jam}}\right)^{\frac{1}{2}}\right]$	Drew (1968)
0	2	$q = v_f \cdot k \cdot \left(1 - \frac{k}{k_{jam}}\right)$	Greenshields (1935)
1	2	$q = v_f \cdot k \cdot \exp \cdot \left(\frac{k}{k_c}\right)$	Edie (1961)
1	3	$q = v_f \cdot k \cdot e^{-\frac{1}{2}\left(\frac{k}{k_c}\right)^2}$	Drake et al. (1967)

The YOLOv4-tiny algorithm (Fig. 4) is created based on the YOLOv4 structure to achieve faster object detection performance. It uses the CSPDarknet53-tiny network as a backbone network. In the YOLOv4-tiny algorithm, the prediction process can be briefly described as follows (Jiang et al., 2020; Zhang et al., 2022; Wang et al., 2021; Wang et al. 2022):

- The input images are adjusted in terms of size;
- The images are subdivided into grids of size S × S;
- Each grid uses B bounding boxes to detect objects;
- The algorithm generates S × S × B bounding boxes, which cover the entire input image;
- If the centre of some object falls in some gird, the bounding boxes in that grid will predict the object;
- To decrease the redundancy of bounding boxes during the prediction process, the confidence threshold is estimated and compared with the confidence score. When the confidence score of a certain bounding box is greater than the confidence threshold, the bounding box is retained; otherwise, it is removed. The confidence score of a bounding box is calculated as follows:

$$C_i^j = P_i^j \times IOU_{pred}^{truth} \quad (10)$$

$$P_i^j = \begin{cases} 0 & \text{no target in the cell} \\ 1 & \text{there are targets in the cell} \end{cases} \quad (11)$$

$$IOU_{pred}^{truth} = \frac{B_{ground\ truth} \cap B_{predicted}}{B_{ground\ truth} \cup B_{predicted}} \quad (12)$$

in which C_i^j is the confidence score of the j-th box in the i-th grid, P_i^j is a function of the object, and IOU_{pred}^{truth} is the so-called intersection over union (IOU). IOU_{pred}^{truth} represents the degree of overlap between the predicted result and the bounding box in the original image. It is the most common indicator in object detection.

When the confidence score is high, the predicted box is close to the ground truth box.

The loss function of YOLOv4-Tiny comprises the confidence loss function ($loss_1$), the classification loss function ($loss_2$) and the bounding box regression loss function ($loss_3$), which can be calculated as follows (Jiang et al., 2020; Zhang et al., 2022):

$$Loss = loss_1 + loss_2 + loss_3 \quad (13)$$

- confidence loss function, $loss_1$:

$$loss_1 = -\sum_{i=0}^{S^2}\sum_{j=0}^{B} W_{ij}^{obj}\left[D_i^j \log\left(C_i^j\right) + \left(1\text{-}D_i^j\right)\log\left(1\text{-}C_i^j\right)\right]$$

$$-\lambda_{noobj}\sum_{i=0}^{S^2}\sum_{j=0}^{B}(1\text{-}W_{ij}^{obj})[D_i^j \log(C_i^j) + (1\text{-}D_i^j)\log(1\text{-}C_i^j)] \quad (14)$$

in which S_2 is the number of grids in the input image, B is the number of the bounding boxes in a grid, and W_{ij}^{obj} is a function of the object. If the j-th bounding box of the i-th grid is responsible for detecting the current object $W_{ij}^{obj} = 1$ otherwise $W_{ij}^{obj} = 0$. In addition, D_i^j and C_i^j are the confidence scores of the predicted box and the confidence score of the truth box respectively and λ_{noobj} is a weight parameter.

- Classification loss function, $loss_2$:

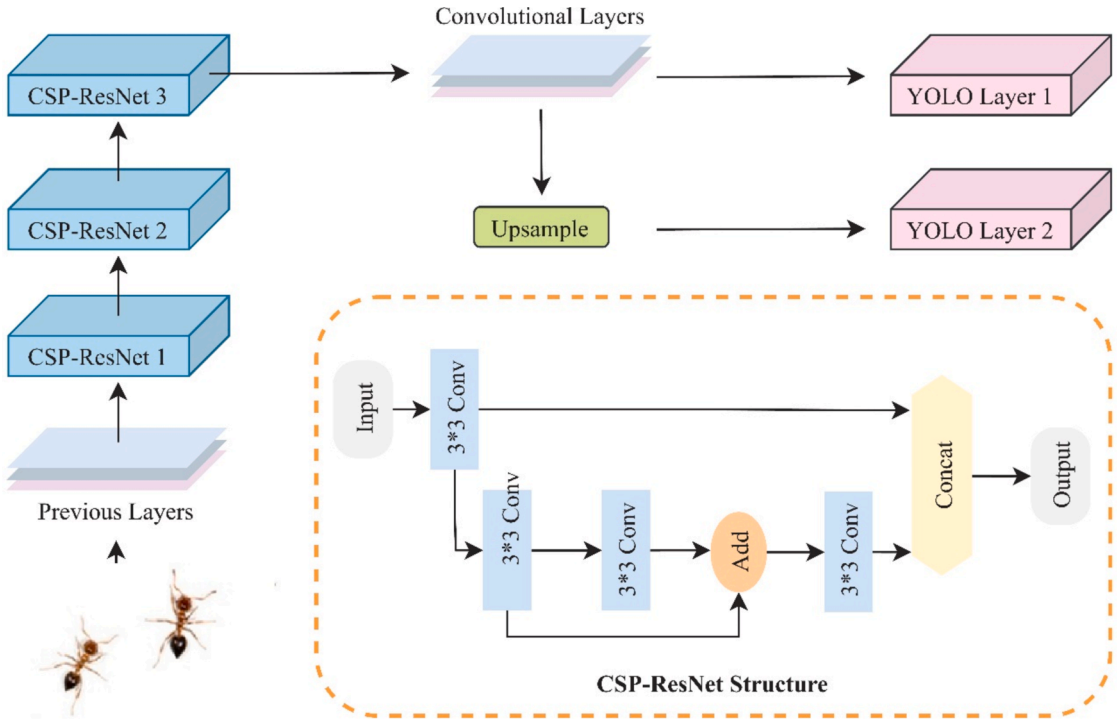

Fig. 4. YOLO v4-tiny structure
(adapted from Wang et al., 2022).

$$loss_2 = -\sum_{i=0}^{S^2}\sum_{j=0}^{B} W_{ij}^{obj}\sum_{c=1}^{C}\left[Q_i^j(c)\log\left(P_i^j(c)\right)-(1-Q_i^j(c)\log\left(1-P_i^j(c)\right)\right] \quad (15)$$

where $P_i^j(c)$ and $Q_i^j(c)$ are the predicted probability and the truth probability to which the object belongs to classification in the bounding box of the grid.

- bounding box regression loss function, $loss_3$:

$$loss_3 = 1 - IOU + \frac{\rho^2(b, b^{gt})}{c^2} + \frac{16}{\pi^4}\cdot\frac{\left(\arctan\frac{w^{gt}}{h^{gt}} - \arctan\frac{w}{h}\right)^4}{1 - IOU + \frac{4}{\pi^2}\cdot\left(\arctan\frac{w^{gt}}{h^{gt}} - \arctan\frac{w}{h}\right)^2} \quad (16)$$

$\rho^2(b, b^{gt})$ denotes the Euclidean distance between the center points of the prediction box and the ground truth box, c is the minimum diagonal distance of the smallest enclosing box covering two boxes, w^{gt} and h^{gt} are the truth width and height of the bounding box, respectively, w and h denote the predicted width and height of the bounding box.

To evaluate the detection performance of the model, numerous metrics, including Precision, Recall, Accuracy and F1 score, can be used:

$$P_r = \frac{TP}{TP + FP} \quad (17)$$

$$R_e = \frac{TP}{TP + FN} \quad (18)$$

$$A_c = \frac{TP + TN}{TP + TN + FP + FN} \quad (19)$$

$$F1 = \frac{2}{\frac{1}{P_r} + \frac{1}{R_e}} = \frac{2\cdot TP}{2TP + FP + FN} \quad (20)$$

In Eqs. (17)-(20), the symbols TP, FN, TN, and FP are the main prediction outcomes and define the True Positive, the False Negative, the True negative and the False Positive, respectively. Table 2 shows the definitions of the four categories.

As for the tracking of ants, any ant that enters an image of the analysed video is considered as a new tracking object, so the method assigns it an identification number and initializes the bounding box for this ant. The linear Kalman filter (Kalman, 1960) is used in this study to reduce noise caused by false detections (Welch and Bishop, 2006). The interested reader can find more details about the Kalman filter and its application in object tracking in (Guerrieri and Parla, 2022). Fig. 5 illustrates the main steps for tracking an ant in successive frames in a video sequence.

3.1. Model training and outcomes

Since no public datasets are available for the studied ant species (Ochetellus), a new dataset named "*Ant Italy*" was created for this research. First, we selected 11,820 ant images from the recorded videos. From this large dataset, a final dataset was created consisting of 8274 images (i.e. 70 % of 11820) for neural network training (with a total of 32,378 annotated bounding boxes of ants) and 3546 images (i.e. 30 % of 11,820) for testing and validation. In this way, the neural network learned a wide range of ant images. The training epoch was set to 180. Fig. 6 illustrates the training epoch loss curve, which indicates a sharp decrease in the first 3 epochs and stabilization after 20 epochs. The values of the metrics (Loss, Precision and Log-average Miss Rate) prove that the training process can detect ants with high accuracy and precision (Fig. 7 and Fig. 8).

Table 2
Metrics and symbols of Eqs. (17)-(20).

Confusion matrix		Ground truth	
		Positive	Negative
Prediction	Positive	TP	FP
	Negative	FN	TN

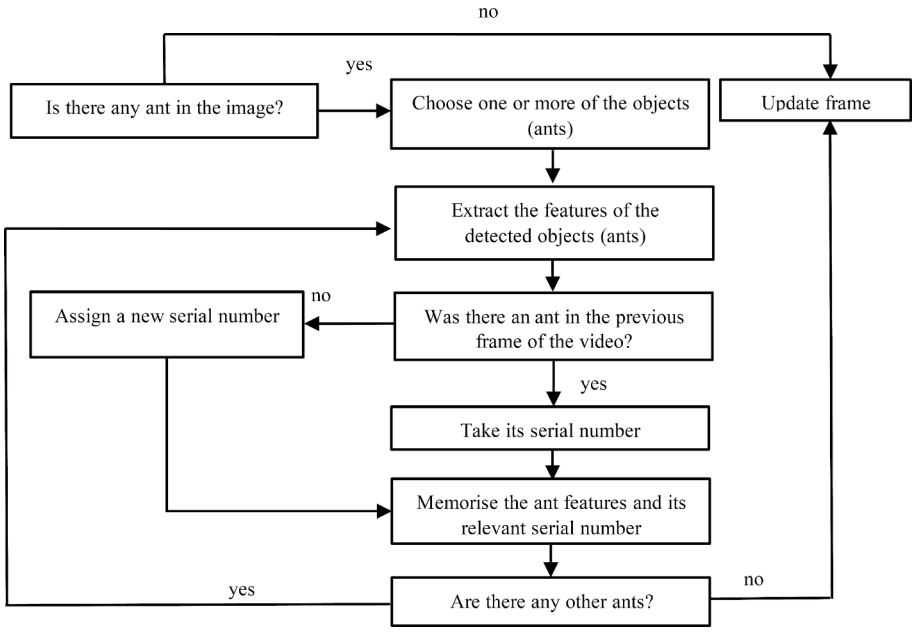

Fig. 5. Steps to tracking an ant in successive frames of a video.

Fig. 6. Loss curve.

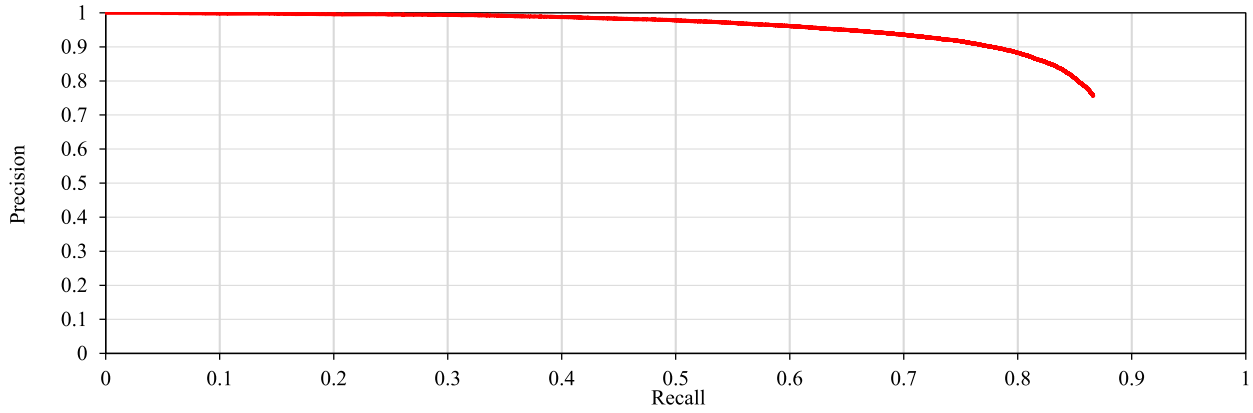

Fig. 7. Precision-Recall curve.

4. Experiments, results and discussion

The experiments refer to a natural trail connecting the nesting site to a lawn with a quasi-smooth surface in an outdoor environment in Italy. We collected qualitative and quantitative traffic data for a single bidirectional traffic stream. The 30 cm section of the trail studied (Fig. 9) has a quasi-constant horizontal alignment during the data collection interval, similar to a static highway section. To reduce complexity, intersections and junctions were excluded from the experiments, as these would be comparable to freeway sections without entrances and exits,

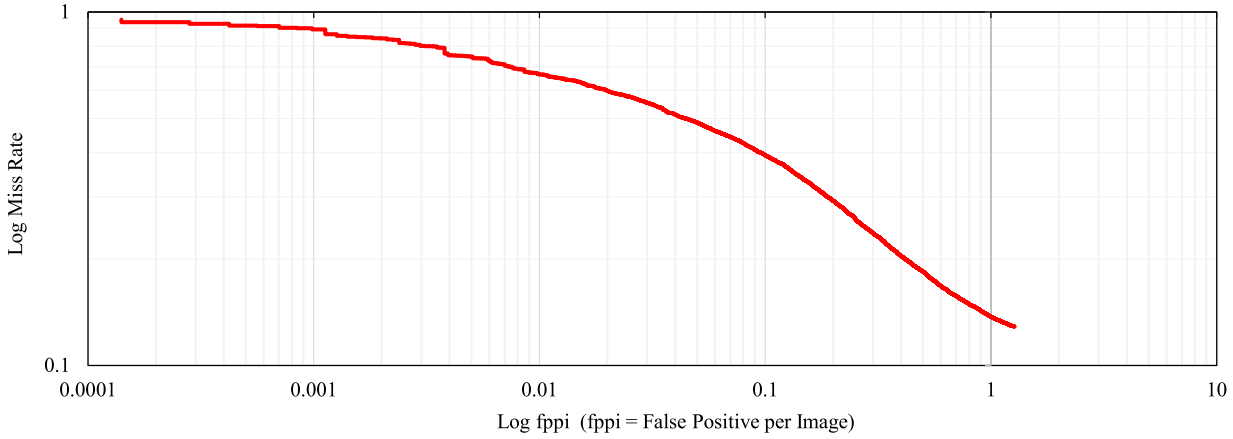

Fig. 8. Miss Rate in function of False Positive per Image.

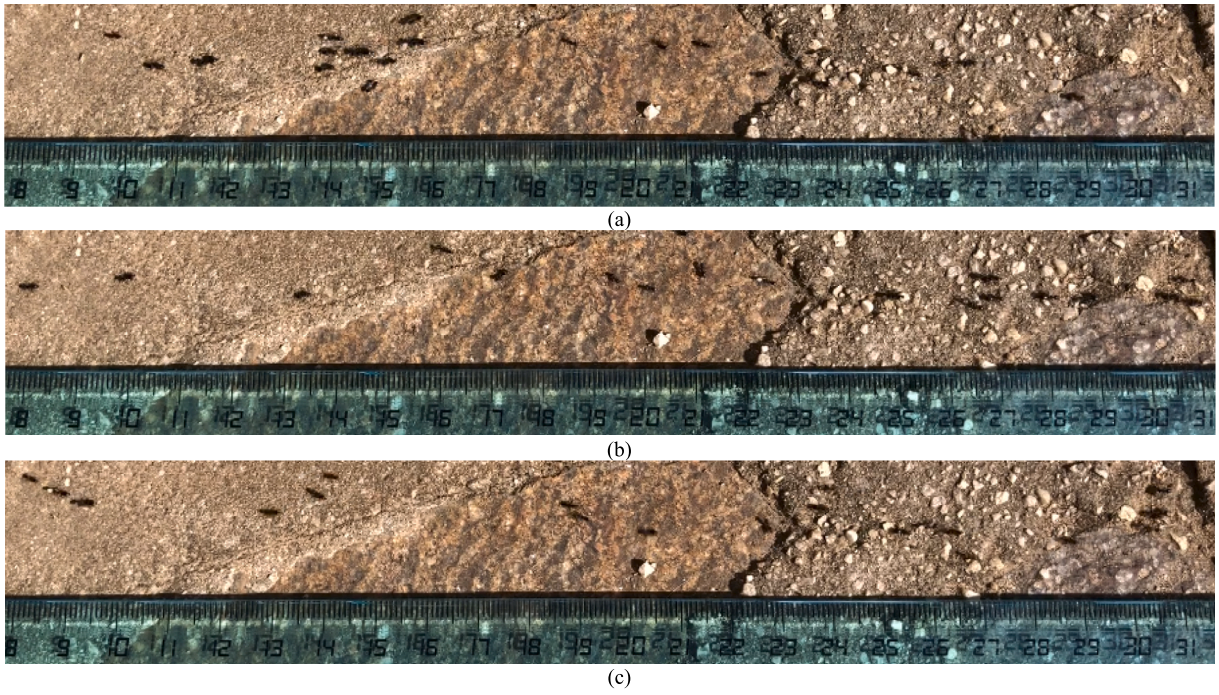

Fig. 9. Snapshots of the observed trail section whose length L ≈ 100·l in the units of the body length of a single ant (l ≈ 3 mm).

which are known to affect traffic density and level of service negatively. We recorded video sequences of oncoming traffic, each lasting 30 s with a resolution of 1334 × 750 pixels at 326 ppi (frame rate of 60 Hz). The time interval between two consecutive videos was 30 s. In total, more than 110 videos of traffic ants were collected (55 for each traffic direction). The ant species under consideration is the Ochetellus (body length: l ≈ 3 mm). This choice guaranteed that all ants have very similar body lengths and perform the same behavioural reactions. Fig. 9 shows photos of the analysed trail section at three different instants of time.

By applying detection and tracking algorithms (cf. Sect. 3), the trajectories, speeds, and accelerations of numerous individuals were estimated along with macroscopic traffic variables (mean speed, density, and flow, cf. Sect. 2) under both undisturbed conditions and disturbed environments created with a repellent substance (citronella oil). Starting from the videos' analysis, each ant's detection was achieved by applying the YOLOv4-Tiny detection algorithm according to the procedure described in the previous sections. The Kalman filter was applied for the tracking processes (Fig. 10) (Meihong et al., 2020).

Fig. 11 shows an example of the temporal-spatial diagram for the studied trail, created using the proposed detection and tracking algorithms (cf. Sect. 3).

We found that when two ants encounter each other, their antennas are often in contact with each other for a certain time interval. In this study, speed reduction during head-on encounters was only analysed qualitatively. However, it is evident that the head-on encounter process between ants involves three distinct phases of motion: the deceleration phase due to encountering each other (from free speed to zero), the stop phase for information exchange, and the acceleration phase back to free speed. In general, the time loss during the deceleration phase is less than that during the acceleration phase (Wang et al., 2018).

As shown in Fig. 3, the temporal-spatial diagram (i.e., the trajectories of the ants, cf. Fig. 11) allows us to estimate the macroscopic traffic variables of flow q, density k, and mean speed v.

In traffic engineering, the relationship between flow and density is the so-called fundamental diagram. In this study, this diagram was estimated from the analysis of videos and plotted in Fig. 12 and the temporal-spatial diagrams (Fig. 11). Instead, Fig. 13 shows the relationships between mean speed-density and flow-density. Scatter plots

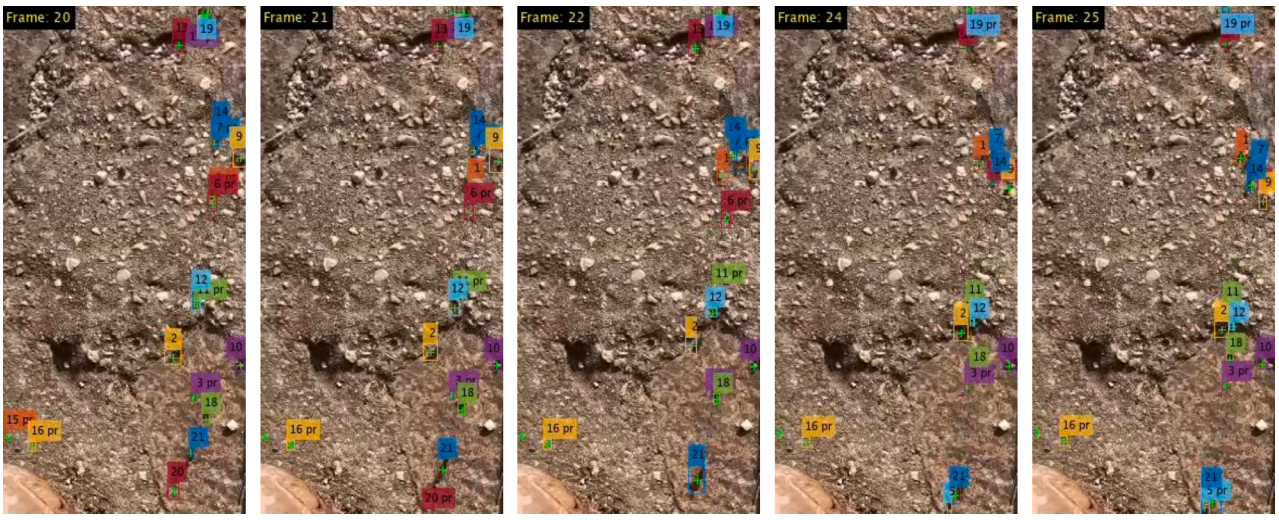

Fig. 10. Examples of ant tracking in four frames of one video.

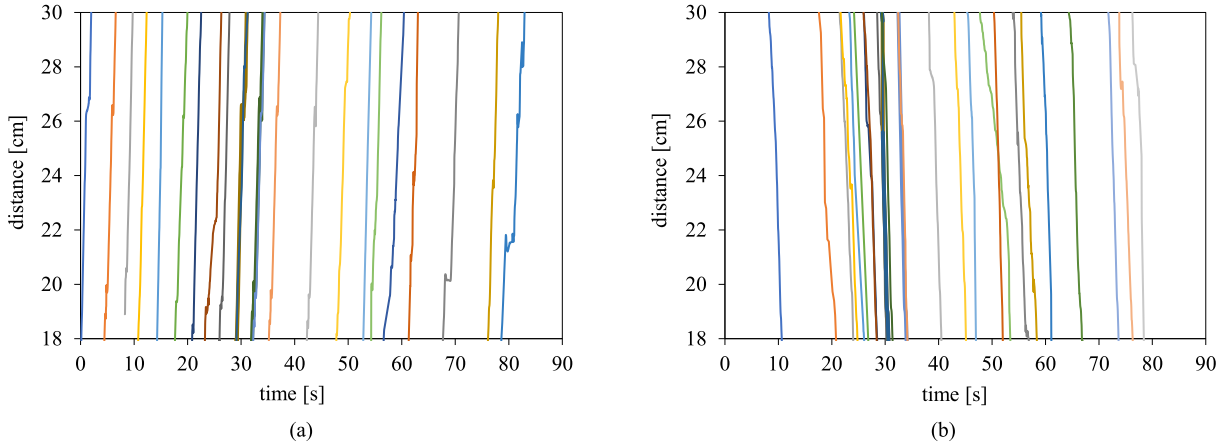

Fig. 11. Examples of temporal-spatial diagrams: a) from cross-section placed at 18 cm to cross-section placed at 30 cm; b) from cross-section placed at 30 cm to cross-section placed at 18 cm (cf. Fig. 9 and Fig. 3).

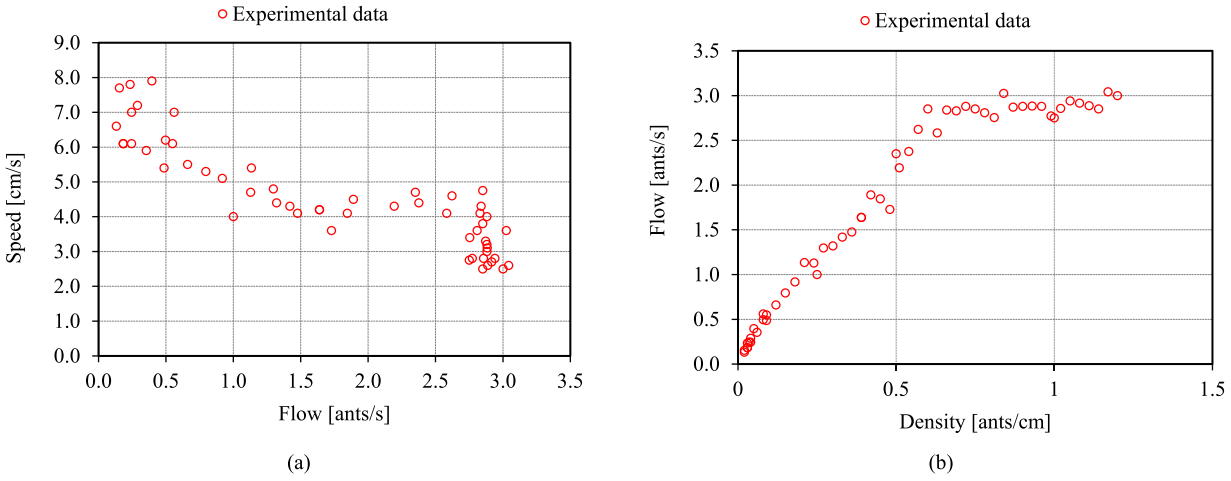

Fig. 12. Speed-flow v = v(q) and Flow-density q = q(k) relationships. Experimental points and theoretical Greenshields model (ant-flow in the direction 1: from the cross-section located at 0 cm to the section located at 30 cm, cf. Fig. 9).

were obtained from successive time intervals $\Delta T_j = 30$ s; the cross section is located at 15 cm (Fig. 9). For each interval of time ΔT_j, flow (q), mean speed (v), and density (k) were calculated using Equations (3), (4), and (5), respectively. A total of 110 pairs of (v; k), (q; k), (v; q) were estimated, as follows: 55 pairs for the flow stream in the direction 1 (from the cross-section located at 0 cm to the cross-section located at 30

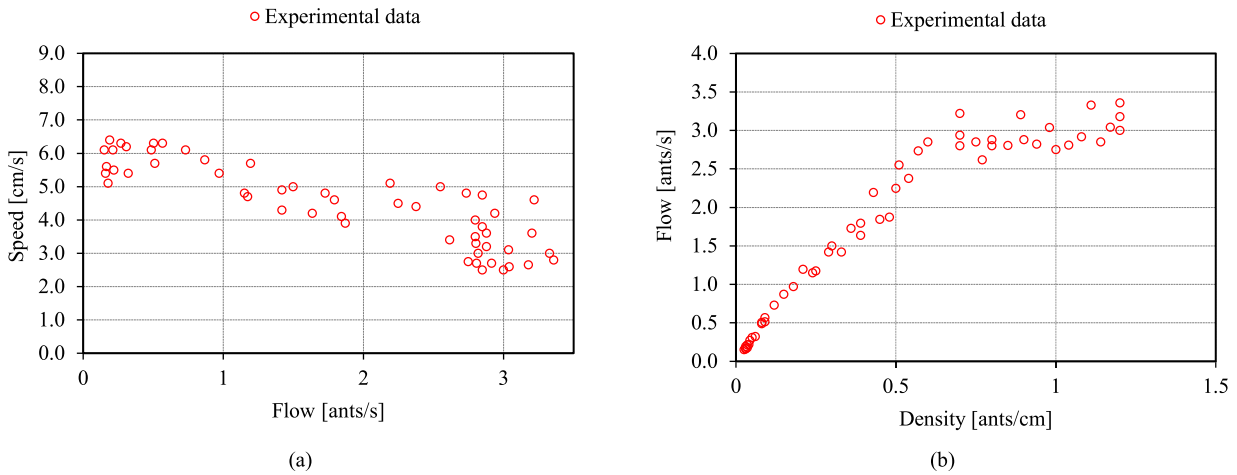

Fig. 13. Speed-flow v = v(q) and Flow-density q = q(k) relationships. Experimental points and theoretical Greenshields model (ant-flow in the direction 2: from the cross-section located at 30 cm to the section located at 0 cm, cf. Fig. 9).

cm) and 55 pairs for the opposite direction.

From Figs. 12 and 13, it can be deduced that the mean speed is almost independent of density, and the flow increases almost linearly with the density up to a certain value, k*.

In general, the theoretical fundamental diagrams for a given cross-section of a highway can be estimated using serval models (Table 1). Most traffic-flow models (Greenshields et al., 1935; Pipes, 1953; Underwood, 1960) show that the mean speed of vehicles decreases non-linearly with density. In particular, in the case of Greenshields' model (cf. Table 1), the relationships between flow (q), speed (v) and density (k) are given by the following equations:

$$v = v_f \cdot e^{-\frac{1}{2}\left(\frac{k}{k_{jam}}\right)^2} \tag{21}$$

$$q = v \cdot \sqrt{\frac{\ln \frac{v_f}{v}}{\frac{0.5}{k_{jam}^2}}} \tag{22}$$

$$q = v_f \cdot k \cdot e^{-\frac{1}{2}\left(\frac{k}{k_{jam}}\right)^2} \tag{23}$$

In which v_f is the free-flow speed and k_{jam} is the jam density.

It is important to note from Fig. 14a that for ant-traffic, the Greenshields model does not fit the experimental data when $k > k_c$, where k_c is the critical density ($k_c \approx 0.6$ ants/cm) related to the capacity c of the traffic stream ($c = q_{max} \approx 3$ ants/s). In addition, the analysis of the experimental data in terms of flow rate q and density k revealed no evidence of jamming (flow does not tend to zero and does not even decrease; after the critical density, it just remains nearly constant), unlike vehicular traffic streams on highways. In fact, the empirical fundamental diagram shows no transition to a jammed phase (John, et al., 2007). In contrast to typical fundamental diagrams observed on highways and other road infrastructures under uninterrupted traffic conditions, we experimented that ant speed appears to be quasi-constant with density (Fig. 13a). This phenomenon is caused by the fact that ants walk within platoons, which reduces the effect of density on the mean speed. As a matter of fact, ants inside a platoon move with almost equal speeds, keeping small time headways h_{si} (cf. Eq. (1), whereas solitary ants can move faster if they perceive an intense pheromone mark produced by a preceding platoon (John et al., 2009). Another way for ants to prevent overcrowding and jamming on a trail is to choose one or more alternative routes. Finally, no overtaking manoeuvres were detected; only occasionally, some ants temporarily left the track and were overtaken by the others.

Given these considerations, a two-phase flow diagram is proposed as depicted in Fig. 14b. In fact, for low-density values, the flow q increases linearly with the density k. In contrast, at high density the flow reaches the maximum value (i.e. the capacity $c = q_{max}$) and remains constant. The diagram can be described as follows:

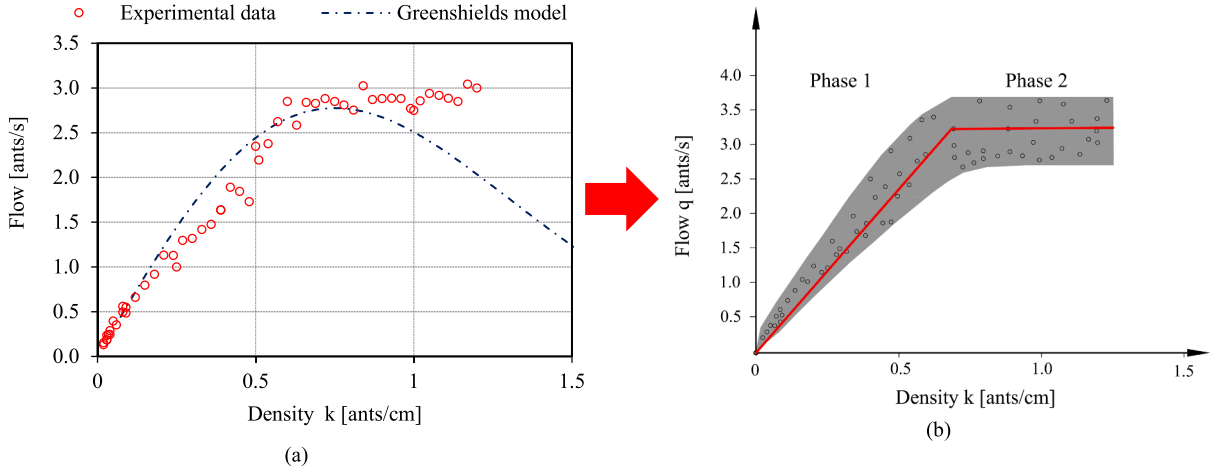

Fig. 14. Experimental flow density data (a) and proposed flow-density diagram (b).

- Phase 1 ($k \leq k_c \approx 0.6$ ants/cm): q increases linearly with k, ants move freely at speed $v = v_f$ (free-flow speed);
- Phase 2 ($k > k_c \approx 0.6$ ants/cm): q stops increasing with k but does not decay as in the case of Greenshields model for vehicular traffic.

A key factor determining the difference between traffic streams on highways and traffic of ants is due to the number of contacts faced with nestmates, which causes several ants to stop and consequently cause the reduction of their average speed, which remains quasi-constant or slightly decreases in the range $0 < q \leq q_{max} = c$ (cfr. Fig. 13a).

In summary, from a macroscopic point of view, in contrast to what is observed in vehicular traffic, in ant-traffic, the flow always increases monotonically with density until the capacity is reached and no jam phenomena are exhibited.

The case study illustrated in this article demonstrates that ants are capable of solving complex traffic regulation problems via relatively simple rules that are not imposed externally and arbitrarily (as in traffic on traditional roads) but that emerge from local direct (ant contacts) or indirect (through a chemical signal) collaborations between individuals. Thus, ants behave more cooperatively than vehicles on conventional roads.

However, from a macroscopic perspective, ants' strategies to maximize traffic flows and prevent jamming can be applied to novel digitalized road infrastructures thanks to emerging technologies such as smart roads and CAVs. Smart roads essentially adopt cooperative technologies of intelligent transport systems (C-ITS) to enable communication and cooperation between all vehicles and between them and the road infrastructure.

Smart roads may employ one or more of the following traffic control systems and devices (Guerrieri, 2021; Ioannou, 2024):

- Lanes for AVs and CAVs;
- Internet of Things (IOT);
- Sensors for monitoring traffic flows, structures (bridges, viaducts etc.), road pavements (Al-Qadi et al., 2004; Praticò et al. 2023), weather and air pollutants;
- Ramp-metering systems;
- Hard Shoulder Running (HSR) systems;
- Variable Speed limits (VSL) (Isaenko et al. 2024) and Variable Message Signs (VMS) (Wu, et al. 2024);
- Green Islands (GIs);
- Electric priority lanes;
- Piezoelectric devices to generate electrical energy;
- Smart street lights (Yoshiura et al., 2013);
- Safety barriers equipped with an accident monitoring system (Dinnella et al., 2020).

Several studies have examined the theoretical impact of CAVs on highway capacity. Using microscopic traffic simulations or analytical models, some studies have estimated an increase in highway lane capacity from 180 % to 500 % (Guerrieri, 2021). However, these studies assumed the fluctuation of vehicle speeds and a confined trial of vehicles inside the carriageway lanes.

Based on the main results of the present research and to avoid congestion, we can assume a very similar traffic regulation process to that of ants for smart roads travelled by CAVs (Fig. 15).

In fact, the communication and cooperation systems of CAVs (i.e. V2V and V2I technologies) enable the exchange of information about the movement between vehicles within the traffic stream, similarly to the exchange of information between ants on a certain chemical trail created by the pheromone which, as mentioned earlier, implies the avoidance of traffic jams.

Therefore, in the case of smart roads and automated highways (Ioannou, 1997), a proper management area (MA) could be used to set a constant speed value for each CAV, corresponding to the maximum speed legally allowed on the highway ($v_i = v_{max} = \text{const.}$). With this hypothesis, one finds that the vehicular flow is increasingly monotonically with the density k of CAVs (Fig. 15):

$$q = v \cdot k = v_{max} \cdot k \tag{24}$$

Eq. (24) substantially corresponds to Phase 1 of the two-phase flow diagram represented in Fig. 14b estimated for ant-traffic.

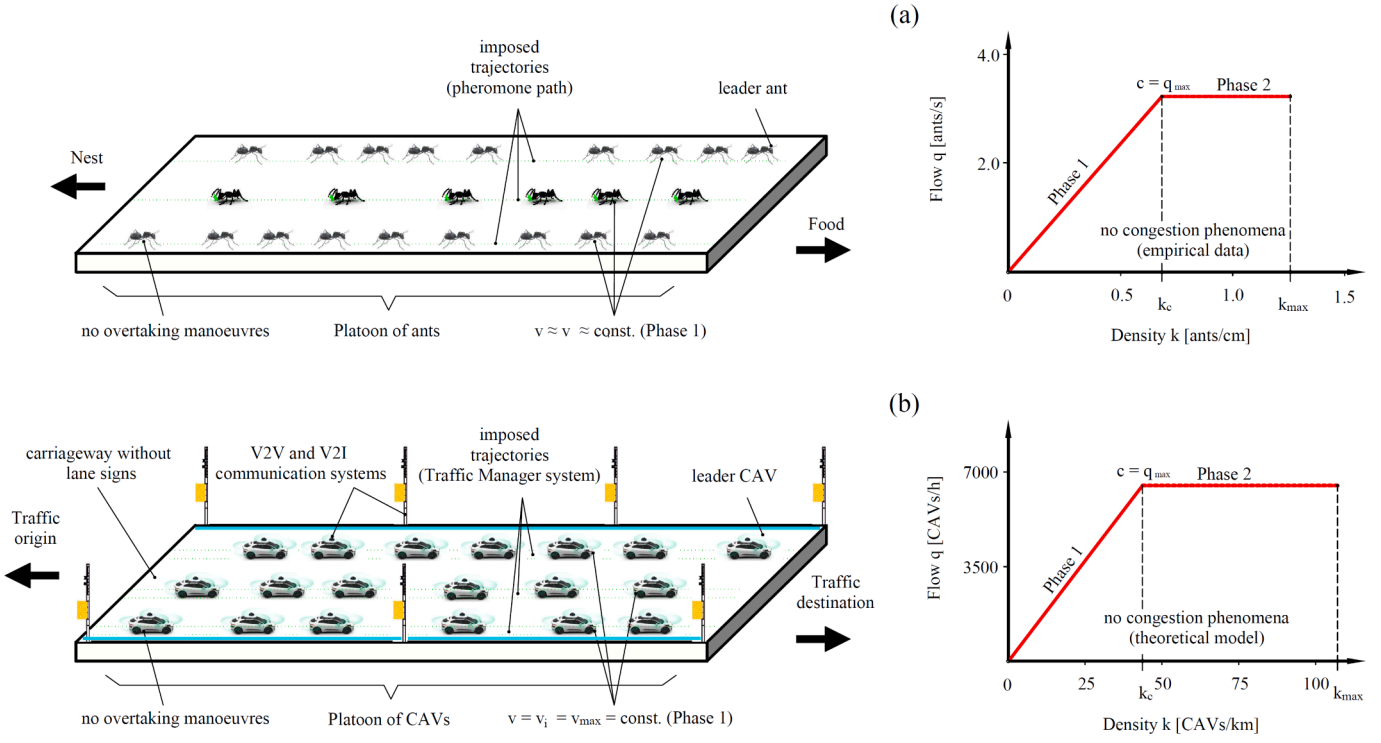

Fig. 15. Scheme of the proposed analogy between the flow of ants (a) and the flow of CAVs on smart roads (b).

Starting from a reasonable lane mean capacity value $c_T = 2000$ veh/h of a traditional highway with traffic steams composed by only human-driving vehicles (HVs), we have estimated the relationships $v = v(q)$, $q = q(k)$ and $v = v(k)$ in the case of a smart road with traffic formed only by CAVs imposing a theoretical stream capacity $c = \alpha \cdot c_T = \alpha \cdot 2000$ veh/h with $\alpha = 1.8–3.2$ (Ioannou, 1997; Guerrieri, 2021) and with three different maximum speed values ($v_{max} = 130$ km/h, $v_{max} = 140$ km/h, $v_{max} = 150$ km/h). Specifically, new communication technologies and cooperative systems applied to infrastructures and vehicles will ensure the maintenance of short headways between CAV_S, which will have a remarkable effect in terms of capacity. For instance, with a minimum mean headway $h^*_{ti} = 0.563$ s, the corresponding capacity is $c = 3600/h^*_{ti} = 3600/0.563 \approx 6400$ CAV_S/h (i.e. the lane capacity obtained by imposing $\alpha = 3.2$ in the previous relation $c = \alpha \cdot c_T$). A total of nine scenarios were analysed, as shown in Table 3. The outcomes of the theoretical model do not show congestion phenomena (Fig. 16) in each traffic stream of the carriageway.

For $k_c \leq k \leq k_{max}$ (Phase 2) $q = c = const.$, v decreases as shown, for example, in Fig. 16 in the case of scenario S 9. Empirical studies on conventional highways have shown maximum densities in the range $k_{max} = 120–160$ veh/km/lane, and these values can also be considered plausible for smart roads. However, to maximize the benefits in terms of travel times, the smart road operator should ensure that the infrastructure preferably operates in phase 1, as this phase determines the maximum permitted speed and consequently reduced travel times. Conversely, in Phase 2 high density values can produce significant and unacceptable mean speeds, even below 60 km/h for $k \approx k_{max}$.

However, unlike conventional highways, where the capacity $c = q_{max}$ is reached at a vehicles mean speed v_c lower than the free-flow speed $v_f = v_{max}$ (e.g. in the Greenshield model $v_c = 0.5\ v_f$), followed by a drastic speed and flow reduction at increasing density, the application of ANTi-JAM solutions, inspired by the ants' behaviour, would allow smart roads to reach capacity c and maximum speed v_{max} simultaneously (final point of phase 1) followed by a unavoidable but moderate speed reduction at constant flow at increasing density (for $k \ll k_{max}$ in Phase 2), with enormous benefits for the transportation system and avoiding congestion phenomena.

It is worth underlining that motorists often choose to follow other vehicles on traditional roads, even at the risk of being stuck in traffic jams. Therefore, to increase the carriageway capacity, lane separation by horizontal lane markings should not be used (Fig. 15b), as in ant trails. The reason is that the traffic management system could prescribe safe vehicle trajectories (Monteiro and Ioannou, 2023) and a variable number of parallel traffic streams depending on traffic demand level to limit the risk of flow instability and congestion.

5. Conclusions

Ants are social insects that communicate with each other primarily through pheromone signals emitted by one ant and that can be picked up by another. Contact is another common method for communicating information of different types. This research uses some traffic engineering methods to analyse traffic flow variables on a bidirectional ant trail in a natural environment. The ant species studied was Ochetellus, whose body length is around 3 mm. We recorded several video sequences of ant-traffic that were 30 s in duration. A Deep learning-based approach and the YOLOv4-tiny detection algorithm were applied to detect and track ants from videos. The estimation of the ant trajectories (space–time diagrams) allowed us to calculate the values of the main macroscopic traffic variables (mean speed v, flow q and density k) for subsequent time intervals, each 30 s long.

From direct observations and traffic datasets related to each unidirectional single-lane trail, several qualitative and quantitative insights were derived, including:

- ants can solve complex traffic control problems by simple rules;
- the relationship between the flow rate q and density k revealed no evidence of jam phenomena;
- in contrast to the typical shape of fundamental diagrams of highways and other road infrastructures under uninterrupted traffic conditions, the mean speed of ants appeared to be quasi-constant with density. In particular, at low ant density, the flow q increases linearly with the density k, whereas at high density, it reaches the maximum value (i.e. the capacity) and remains constant;
- spatial distribution of individuals along the trail shows that ants move predominantly in platoons;
- within each platoon, ants maintain almost equal speed, keeping small time headways;
- no overtaking maneuvers are performed.

Major findings of the study

We formulate a set of rules and potential analogies between the future traffic regulation of cooperative and automated vehicles (CAVs) on smart roads and the organization of ant traffic. These analogies arise from the consideration that in smart roads, communication and cooperation systems (i.e. V2V and V2I), will allow CAVs to exchange information about the movement within traffic streams in a very similar way to the information exchange adopted by ants within a given pheromone trail. Therefore, a traffic management area (MA) could be used to set the speed of each CAV to a value equal to the maximum speed allowed on the highway, and platoons could be artificially formed by setting small mean headways (h^*_{ti}) between vehicles.

To estimate the effect of a traffic regulation inspired by the ants' behaviour, this research considered numerous traffic scenarios that differ from each other in the following characteristics: maximum speed ($v_{max} = 130$ km/h, $v_{max} = 140$ km/h, $v_{max} = 150$ km/h) and lane capacity values obtained by varying the h^*_{ti} values.

The first results of the proposed theoretical model reveal that, as in ant-traffic, in smart roads, the traffic flows increasingly monotonically with the density k without apparent congestion phenomena, up to a nearly constant/maximal value. To maximize the benefits in terms of travel times and, therefore, transport users' satisfaction, the smart road should preferably operate in phase 1 of the fundamental diagram – with density values less than the critical density k_c – because this traffic condition produces the maximum permitted speed.

Therefore, using ANTi-JAM strategies, inspired by the ants' collective motion, could allow the simultaneous obtaining of capacity c and maximum speed v_{max}, with remarkable benefits for the transportation

Table 3
Scenarios and traffic variable values considered for phase 1 of smart roads with traffic composed only of CAVs.

Scenario									
Traffic flow variable	S 1	S 2	S 3	S 4	S 5	S 6	S 7	S 8	S 9
v_{max} [km/h]	130	130	130	140	140	140	150	150	150
$\alpha = c / c_T$	≤ 1.8	1.8–2.5	2.6–3.2	≤ 1.8	1.8–2.5	2.6–3.2	≤ 1.8	1.8–2.5	2.6–3.2
k[CAVs/km]	≤ 28	29–38	39–49.2	≤ 28	29–38	39–45.7	≤ 28	29–38	39–42.7
c [CAVs/h]	≤ 3640	3641–4940	4941–6400	≤ 3920	3921–5320	5321–6400	≤ 4200	4201–5700	5701–6400
h^*_{ti}[s]	≥ 0.99	0.99–0.73	0.73–0.56	≥ 0.92	0.92–0.68	0.68–0.56	≥ 0.88	0.88–0.63	0.63–0.56

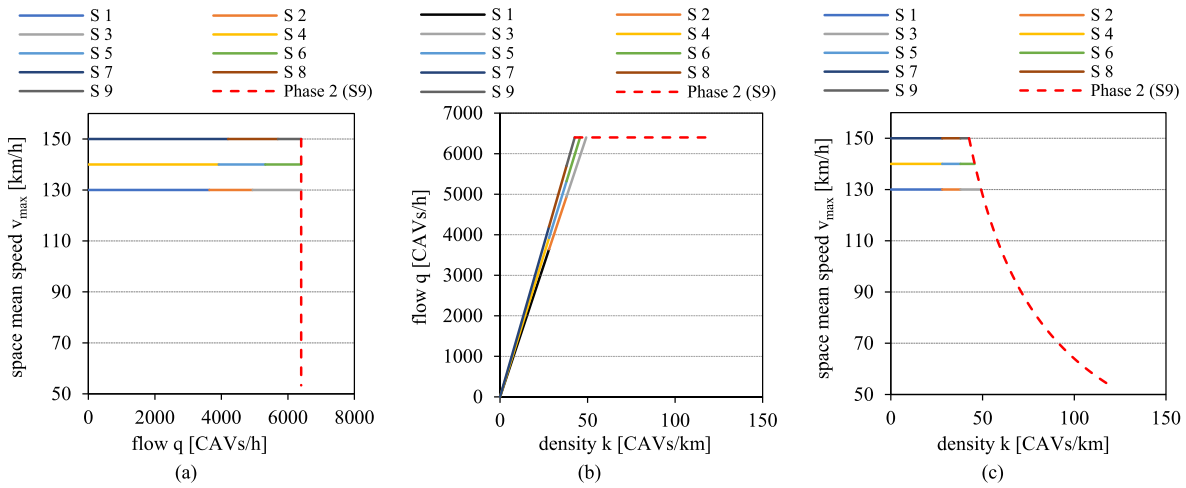

Fig. 16. v = v(q), q = q(k) and v = v(k) relationships obtained for the scenarios of Table 3 (the dotted lines denote the Phase 2 for the scenario S 9).

system and avoiding congestion phenomena.

Limitations of the study

This research has its own limitations, which are encountered at various stages. The major limitation is that traffic data collection includes only one ant species. Given this limitation, it is not possible to generalize the results from this study to all ant species. Another limitation is related to the analysis of a single trail section without curves, intersections and conflict areas among several ants' streams. Finally, CAVs are emerging technologies and no empirical data are available from real-world applications in traffic and highway engineering.

Research perspectives

Studies on the collective motion of ants offer plenty of opportunities and information for testing models aimed at identifying strategies for better traffic regulation of future digitized infrastructures (smart roads).

However, despite these promising findings, further studies are needed to establish more accurate traffic models and rules that reflect the behaviour of ants and their abilities to avoid congestion on smart roads and thereby maximize both vehicle density and infrastructure capacity.

CRediT authorship contribution statement

Marco Guerrieri: Writing – original draft, Visualization, Methodology, Investigation, Formal analysis, Data curation, Conceptualization. **Nicola Pugno:** Visualization, Validation, Supervision, Formal analysis, Conceptualization.

Declaration of competing interest

The authors declare that they have no known competing financial interests or personal relationships that could have appeared to influence the work reported in this paper.

Acknowledgements

The authors thank Prof. Raffaele Mauro for having suggested the collaboration between the two authors, the first expert in traffic engineering and the second expert in bioinspired mechanics, merging here for the first time their competences.

The authors acknowledge the Italian Ministry of Universities and Research (MUR), in the framework of the project DICAM-EXC (Departments of Excellence 2023-2027, grant L232/2016).

Data availability

No data was used for the research described in the article.

References

Al-Qadi, I.L., Loulizi, A., Elseifi, M., Lahouar, S. 2004. The Virginia smart road: the impact of pavement instrumentation on understanding pavement performance. Asphalt Paving Technology: Association of Asphalt Paving Technologists-Proceedings of the Technical Sessions, 73, 427–465.

Bekey, G.A., Burnham, G., Seo, J., 1977. Control theoretic models of human drivers in car following. Hum. Factors. 19 (4), 399–413.

Billen, J., Morgan, E. D., 1998. Pheromone communication in social insects sources and secretions. In Pheromone communication in Social Insects: Ants, Wasps, Bees and Termites (ed. R. K. Vander Meer, M. D. Breed, K. E. Espelie and M. L. Winston), pp. 3-33. Boulder, CO: Westview Press.

Bonabeau, E., Dorigo, M., Theraulaz, G., 2000. Inspiration for optimization from social insect behaviour. Nature 400, 39–42.

Couzin, D., Franks, N.R., 2003. Self-organized lane formation and optimized traffic flow in army ants. Proc. r. Soc. Lond. B 270 (139–146), 139. https://doi.org/10.1098/rspb.2002.2210.

Dinnella, N., Chiappone, S., Guerrieri, M., 2020. The innovative "NDBA" concrete safety barrier able to withstand two subsequent TB81 crash tests. Eng. Fail. Anal. 115, 104660.

Elgendy, M., 2020. Deep Learning for Vision Systems; Simon and Schuster: New York, NY, USA.

Fourcassié, N., Dussutour, A., Deneubourg, J.L., 2010. Ant traffic rules. J. Exp. Biol. 213, 2357–2363. https://doi.org/10.1242/jeb.031237.

Gabard. J. F., Henry, J. J., Tuffal, J., David. Y., 1982. Traffic responsive or adaptive fixed time policies? A critical analysis with SITRA-B. Proc. Int. Conf. Road Traffic Signalling. Institution of Electrical Engineers. London.

Gallelli, V., Iuele, T., Vaiana, R., 2016. Conversion of a semi-two lanes roundabout into a turbo-roundabout: a performance comparison. Procedia Comput. Sci. 83, 393–400.

Gallelli, V., Vaiana, R., 2019. Safety improvements by converting a standard roundabout with unbalanced flow distribution into an egg turbo roundabout: simulation approach to a case study. Sustainability (switzerland) 11 (2), 466.

Gallotti, R., Chialvo, D.R., 2018. How ants move: individual and collective scaling properties. J. R. Soc. Interface 15 (143).

Gipps, P.G., 1981. A behavioural car-following model for computer simulation. Tramp. Res. B 15, 105–111.

Grevé, M.E., Bláha, S., Teuber, J., Rothmaier, M., Feldhaar, H., 2019. The effect of ground surface rugosity on ant running speed is speciesspecific rather than size dependent. Insect. Soc. 66, 355–364.

Guerrieri, M., 2021. Smart roads geometric design criteria and capacity estimation based on AV and CAV emerging technologies. A case study in the trans-European transport network. Int. J. Intell. Transp. Syst. Res. 19 (2), 429–440.

Guerrieri, M., Parla, G., 2022. Flexible and stone pavements distress detection and measurement by deep learning and low-cost detection devices. Eng. Fail. Anal. 141, 106714.

Guerrieri, M., Corriere, F., Parla, G., 2013a. Estimation of pollutant emissions from road traffic by image processing techniques: a case study in a suburban area. ARPN J. Eng. Appl. Sci. 8 (8), 668–676.

Guerrieri, M., Parla, G., Corriere, F., 2013b. A new methodology to estimate deformation of longitudinal safety barriers. ARPN J. Eng. Appl. Sci. 8 (9), 763–769.

Guerrieri, M., Corriere, F., Lo Casto, B., Rizzo, G., 2015. A model for evaluating the environmental and functional benefits of innovative roundabouts. Transp. Res. Part D: Transp. Environ. 39, 1–16.
Helly. W., 1961. Simulation of bottlenecks in single-lane traffic flow. In: Herman R C (ed.) Theory of Traffic Flow. Proc. Symp. Theory of Traffic Flow. Elsevier. Amsterdam.
Holldobler B., Wilson, O., 1990. The Ants. Cambridge, Belknap.
Ioannou, P., 1997. Automated Highway Systems. Springer.
Ioannou, P., 2024. Connectivity, automation and safety in transportation of the future. IEEE Trans. Intell. Transp. Syst. 25 (4), 94–123.
Isaenko, N., Colombaroni, C., Fusco, G., Lahijanian, Z., 2024. Statistical and clustering-based assessment of variable speed limits effects on motorway performance from real-world observations. Future Transport. 4 (2), 409–428.
Jiang, Z., Zhao, L., Li, S., Jia, Y., 2020. Real-time object detection method for embedded devices. Comput. vis. Pattern Recognit. 14, 4244.
John, A., Schadschneider, A., Nishinari, K., Chowdhury, D., 2007. Traffic flow on ant trails: Empirical results vs. theoretical predictions. Traffic and Granular Flow, 701–706.
John, A., Schadschneider, A., Chowdhury, D., Nishinari, K., 2008. Characteristics of Ant-Inspired Traffic Flow. Applying the social insect metaphor to traffic models. Swarm Intell. 2, 25–41.
John, A., Schadschneider, A., Chowdhury, D., Nishinari, K., 2009. Traffic like collective movement of ants on trails: absence of a jammed phase. Phys. Rev. Lett. 102 (10), 108001.
Kalman, R.E., 1960. A new approach to linear filtering and predictions problems. J. Basic Eng. 82 (D), 35–45.
Li, F., Liu, Z., Shen, W., Sun, F., Lan, P., 2021. A remote sensing and airborne edge-computing based detection system for pine wilt disease. IEEE Access 9.
Liu, X., Xing, Z., Liu, H., Peng, H., Xu, H., Yuan, J., Gou, Z., 2022. Combination of UAV and Raspberry Pi 4B: Airspace detection of red imported fire ant nests using an improved YOLOv4 model. Math. Biosci. Eng. 19 (12), 13582–13606.
Mauro, R., 2014. Traffic and Random Processes: An Introduction. Springer.
Meihong Wu, Xiaoyan Cao, Shihui Guo., 2020. Accurate detection and tracking of ants in indoor and outdoor environments. bioRxiv .11.30.403816, 2020. doi: https://doi.org/10.1101/2020.11.30.403816.
Monteiro, F.V., Ioannou, P., 2023. Safe autonomous lane changes and impact on traffic flow in a connected vehicle environment. Transp. Res. Part C Emerging Technol. 2023 (151), 104138.
Nishinari, K., Sugawara, K., Kazama, T., Schadschneider, A., Chowdhury, D., 2006. Modelling of self-driven particles: foraging ants and pedestrians. Phys. A 372, 132–141.
Papageorgiou, M., 1991. Concise Encyclopedia of Traffic & Transportation. Pergamon Press.
Peters, K., Johansson, A., Dussutour, A., Helbing, D., 2006. Analytical and numerical investigation of ant behavior under crowded conditions. Adv. Complex Syst. 9, 337–352.
Poissonnier, L.-A., Motsch, S., Gautrais, J., Buhl, J., Dussutour, A., 2019. Experimental investigation of ant traffic under crowded conditions. eLife, 8, art. no. e48945.
Praticò, F.G., Perri, G., De Rose, M., Vaiana, R., 2023. Comparing bio-binders, rubberised asphalts, and traditional pavement technologies. Constr. Build. Mater. 400, 132813.
Redmon, J.; Divvala, S.; Girshick, R.; Farhadi, A., 2016. You only look once: Unified, real-time object detection. In Proceedings of the 2016 IEEE Conference on Computer Vision and Pattern Recognition, Las Vegas, NV, USA, 27–30 June 2016, 779–788.
Reinhardt, L., Blickhan, R., 2014. Level locomotion in wood ants: evidence grounded running. J Exp Biol 217, 2358–2370. https://doi.org/10.1242/jeb.098426.
Schadschneider, D., Chowdhury, K.N., 2011. Stochastic Transport in Complex Systems From Molecules to Vehicles. Elsevier, 10.1007/s00040-019-00694-z.
Vidyarthi, A., Coxon, S., Napper, R., Gusheh, M., 2023. A proposed hierarchy of smart roads: assisting future technological developments. Smart Innovat., Syst. Technol. 342, 455–466.
Wang, G., Ding, H., Li, B., Nie, R., Zhao, Y., 2022. Trident-YOLO: improving the precision and speed of mobile device object detection. IET Image Proc. 16 (1), 145–157.
Wang, S., Song, S., 2016. Experimental study of ant movement in a straight passageway under stress conditions. J. Insect. Behav. 29, 735–743. https://doi.org/10.1007/s10905-016-9593-x.
Wang, Q., Song, W., Zhang, J., Lo, S., 2018. Bi-directional movement characteristics of Camponotus japonicus ants during nest relocation. J. Exp. Biol. 221, jeb181669. https://doi.org/10.1242/jeb.181669.
Wang, Z., Wu, Y., Yang, L., Thirunavukarasu, A., Evison, C., Zhao, Y., 2021. Fast personal protective equipment detection for real construction sites using deep learning approaches). Sensors 21 (10), 3478.
Terven, J., Córdova-Esparza, D.M., 2024. A Comprehensive Review of YOLO: From YOLOv1 and Beyond. ACM COMPUTING SURVEYS. https://doi.org/10.48550/arXiv.2304.0050.
Welch, G., Bishop, G. 2006. An Introduction to the Kalman Filter. Department of Computer Science University of North Carolina at Chapel Hill Chapel Hill, NC 27599-3175. Available: https://www.cs.unc.edu/~welch/kalman/kalmanIntro.html (accessed on 13 December 2024).
Wu, Y., Liu, J., Zhang, N., Rong, J., 2024. Effectiveness, influence mechanism and optimization strategies of variable message Sign: a systematic review. Transport. Res. F: Traffic Psychol. Behav. 105, 116–137.
Yoshiura, N., Fujii, Y., Ohta, N. 2013. Smart street light system looking like usual street lights based on sensor networks. 13th International Symposium on Communications and Information Technologies: Communication and Information Technology for New Life Style Beyond the Cloud, ISCIT 2013, 633–637, 6645937.
Zhang, Y., Yu, J., Chen, Y., Yang, W., Zhang, W., He, Y., 2022. Real-time strawberry detection using deep neural networks on embedded system (rtsd-net): An edge AI application. Comput. Electron. Agric. 192. https://doi.org/10.1016/j.compag.2021.106586.
Zheng, Z., Wang, P., Liu, W., Li, J., Ye, R., Ren, D. 2019. Distance-IoU Loss: Faster and Better Learning for Bounding Box Regression. arXiv:1911.08287 [cs], Nov.
Zollikofer, C.P.E., 1994. Stepping patterns in ants—Part I—influence of speed and curvature. J. Exp. Biol. 192, 119–127.